# circEFR3A promotes breast cancer progression by sponging miR-590-3p to upregulate androgen receptor expression

YUNZHE MI[1*], XINLE WANG[1*], HAN SONG[2], ZHENYU WU[3], SAINAN LI[1], FEI LIU[4], WEI LIU[5], MEIXIANG SANG[4] and CUIZHI GENG[1]

[1]Breast Center, The Fourth Hospital of Hebei Medical University, Hebei Medical University, Shijiazhuang, Hebei 050017, P.R. China; [2]Core Facilities and Centers, Institute of Medical and Health Science, Hebei Medical University, Shijiazhuang, Hebei 050017, P.R. China; [3]Department of General Surgery, Hebei Key Laboratory of Colorectal Cancer Precision Diagnosis and Treatment, The First Hospital of Hebei Medical University, Shijiazhuang, Hebei 050031, P.R. China; [4]Research Center, The Fourth Hospital of Hebei Medical University, Shijiazhuang, Hebei 050017, P.R. China; [5]Department of Breast Surgery, The Fourth Hospital of Shijiazhuang City, Shijiazhuang, Hebei 050000, P.R. China

Received March 7, 2025; Accepted June 19, 2025

DOI: 10.3892/ol.2025.15192

**Abstract.** Circular (circ)RNA, a type of non-coding RNA, serves a critical role in several diseases, including cancer. The present study aimed to elucidate the involvement of hsa_circ_0006522 (circEFR3A) in the advancement of breast cancer (BC) and uncover the molecular mechanisms behind its function. Fluorescence *in situ* hybridization (FISH) was performed on a tissue microarray to assess the expression and intracellular localization of circEFR3A. Kaplan-Meier analysis and Cox proportional hazards model were utilized to evaluate the potential prognostic significance of circEFR3A in relation to the overall survival of patients with BC. The biological function was assessed through gain- and loss-of-function experiments. In addition, dual luciferase reporter assays, RNA immunoprecipitation, FISH and western blotting were performed to identify the interaction between circEFR3A, microRNA (miR)-590-3p and androgen receptors (ARs). Rescue experiments were performed to identify the hypothetical regulatory role of circEFR3A on BC progression *in vivo* and *in vitro*. The results of the present study demonstrated that circEFR3A was significantly upregulated in BC tissues and was associated with a poor prognosis in patients. Findings from the Cell Counting Kit-8, colony formation and Transwell assays revealed that increased circEFR3A expression notably promoted BC cell proliferation, invasion and migration, as well as tumor growth *in vivo*. Mechanistically, circEFR3A was demonstrated to act as a molecular sponge for miR-590-3p *in vitro* and *in vivo*, thereby regulating AR expression and functioning as an oncogene. In summary, the findings of the present study indicate that circEFR3A acts as a novel oncogene in BC by sponging miR-590-3p, leading to the upregulation of AR expression and consequently driving BC progression.

## Introduction

In 2020, there were ~2.26 million new cases of breast cancer (BC) worldwide, making it the most common malignant tumor globally, and for the first time, surpassing lung cancer. Moreover, the incidence rate of BC continues to rise at a rate of 0.6-1% (1,2). BC development and progression involve complex pathological mechanisms, and due to the heterogeneous nature of BC, certain patients do not respond effectively to the current standard treatments (3). An increasing number of studies have reported that several molecules, including non-coding (nc) RNAs, serve essential roles in these processes (4). Therefore, investigating the molecular mechanisms underlying BC progression and identifying new targets for prognosis and molecular therapy are crucial for improving the survival rates of patients with BC.

Circular (circ)RNAs are a type of RNA with a unique closed-loop configuration, distinguishing them from other RNA types by the absence of both a 5' cap and a 3' poly(A) tail. Due to this closed-loop architecture, circRNAs are resistant to exonuclease RNase R digestion. This ensures their stable expression within cells, allowing them to serve a long-term role in transcriptional regulation (5,6). The application of high-throughput RNA sequencing (RNA-Seq) technology has led to the identification of an increasing number of circRNAs. Previous studies have reported that circRNAs can influence tumor progression through ~4 mechanisms, including: i) Acting as sponges for microRNAs (miRNAs/miRs); ii) interacting with proteins; iii) translating polypeptides or

*Correspondence to:* Professor Cuizhi Geng, Breast Center, The Fourth Hospital of Hebei Medical University, Hebei Medical University, 12 Jiankang Road, Shijiazhuang, Hebei 050017, P.R. China
E-mail: 46300349@hebmu.edu.cn

*Contributed equally

*Key words:* circEFR3A, breast cancer, microRNA-590-3p, androgen receptor

proteins; and iv) modulating gene transcription and splicing processes (7-10).

Recent studies have reported the diverse functions of circRNAs in the development and progression of BC (11-15). Certain circRNAs, derived from exons and highly expressed in BC cells and tissues, such as circCDYL, circKIF4A, circBCBM1, circNF1 and circEGFR, are enriched in miRNA response elements (16-20). These circRNAs can act as miRNA sponges by utilizing competitive endogenous (ce)RNA mechanisms. They bind miRNAs in a competitive manner, which results in the increased expression of their downstream target genes. In the present study, the functional role of the circRNA circEFR3A (hsa_circ_0006522) was assessed. The present study aimed to investigate the role of circEFR3A in BC progression. Specifically, the relationship between circEFR3A expression and BC prognosis was assessed, and its potential mechanisms in promoting BC cell proliferation, migration and invasion were examined. To achieve these objectives, various methods were used, including the analysis of circEFR3A expression levels in BC tissues and the assessment of its effects on BC cell behavior. Additionally, the interaction between circEFR3A and miR-590-3p, and its impact on androgen receptor (AR) expression, a target of miR-590-3p, was explored.

## Materials and methods

*Clinical tissue chip array samples*. A tissue microarry (cat. no. HBreD129Su01) with BC tissue samples from 129 patients was purchased from Shanghai Outdo Biotech Co., Ltd. Clinicopathological characteristics and patient survival information were obtained from follow-up records. At the end of the experiment, the slides were scanned using a NanoZoomer 2.0 HT slide scanner (Hamamatsu Photonics K.K.). The study methods adhered to the guidelines of the Declaration of Helsinki and received approval from the Ethics Committee of The Fourth Hospital of Hebei Medical University (approval no. 2024KS189; Shijiazhuang, China).

*Cell culture*. The human BC cell lines MDA-MB-231 (RRID: CVCL_0062), MDA-MB-453 (RRID: CVCL_0419), SK-BR3 (RRID: CVCL_0033), MCF-7 (RRID: CVCL_0031) and BT-549 (RRID: CVCL_1092) were purchased from Procell Life Science & Technology Co., Ltd. and stored in the laboratory. All cell lines were verified within the previous 3 years via short tandem repeat analysis. SK-BR-3 cells were maintained in McCoy's 5A medium (Gibco; Thermo Fisher Scientific, Inc.) with 10% FBS, whilst MDA-MB-231, BT-549 and MDA-MB-453 cells were cultured in RPMI 1640 containing 10% heat-inactivated FBS (Gibco; Thermo Fisher Scientific, Inc.). All cell lines were confirmed mycoplasma-free and incubated at 37˚C with 5% $CO_2$.

*Cell transfection*. The circEFR3A expression plasmid and control constructs were sourced from Guangzhou Geneseed Biotech, Co., Ltd. In addition, circEFR3A small interfering (si)RNA (sense: 5'-CAUUCAGGAGUAUGCUGCU-3'; antisense: 5'-AGCAGCAUACUCCUGAAUG-3') and the control (sense: 5'-CGUACGCGGAAUACUUCGA-3'; antisense: 5'-UCGAAGUAUUCCGCGUACG-3'), the miR-590-3p mimics (cat. no. miR10004801-1-5), miRNA mimic negative control (NC; cat. no. miR1N0000001-1-5), miR-590-3p inhibitors (cat. no. miR20004801-1-5) and miRNA inhibitors NC (cat. no. miR2N0000001-1-5) were purchased from Guangzhou RiboBio Co., Ltd. MDA-MB-231 and MDA-MB-453 cells were independently transfected with miR-590-3P mimics and inhibitors, respectively, using HiPerFect Transfection Reagent (cat. no. 301705; Qiagen, Inc.) at 37˚C for 6 h. Subsequent experiments were performed 48 h post-transfection. Both cell lines received a standardized final concentration of 50 nM miRNA constructs, diluted in serum-free medium according to the manufacturer's optimized protocol.

For siRNA and overexpression plasmid transfection, MDA-MB-453 cells were transfected using FuGENE® HD Transfection Reagent (cat. no. E2311; Promega Corporation), whereas MDA-MB-231 cells were transfected with HiPerFect Transfection Reagent, following the manufacturers' instructions at 37˚C for 6 h. Subsequent experiments were typically performed 48-72 h post-transfection for RNA/protein analysis, with functional assays conducted within 24-96 h.

*Animal experiments*. For the mouse xenograft tumor model, a total of 12 female BALB/c nude mice (age, 4 weeks; weighing, 18-20 g; purchased from Beijing HFK Bioscience Co., Ltd.) were housed under specific pathogen-free conditions at 22±1˚C with 50±5% relative humidity, maintained under a 12-h light/dark cycle (lights on at 7:00 AM) with *ad libitum* access to autoclaved standard chow and sterile water. Each mouse was subcutaneously injected into the right flank with $5x10^6$ MDA-MB-453 cells that had been previously infected with either the pLC5-ciR vector or circEFR3A cells in 200 $\mu$l PBS. On day 9, mice received intratumoral injections of either miR-590-3p mimic or NC at a dose of 5 nmol/injection in 50 $\mu$l PBS. Injections were administered every 3 days for a total of six treatments. Tumor volumes were measured and recorded at each injection point. At the end of the experiment, all mice were euthanized using $CO_2$ delivered at a volume displacement of 30% vol/min (achieved by a flow rate of 1.5 l/min into a 5 l sealed chamber). After 5 min of continuous exposure, death was confirmed by cervical dislocation. Following euthanasia of all mice, tumor weight was analyzed. The animal experiments in the present study were approved by the Ethics Committee of The Fourth Hospital of Hebei Medical University (approval no. 2023016).

*DNA and RNA extraction*. Genomic DNA was isolated from MDA-MB-231 cell using a commercial DNA extraction kit (cat. no. DP304; Tiangen Biotech Co., Ltd.) following the manufacturer's instructions. Total RNA was extracted from the same cells using TRIzol™ reagent (Invitrogen™; Thermo Fisher Scientific, Inc.) according to standard procedures.

*RNase R treatment*. Total RNA was treated with RNase R from *E. coli* (Epicentre; Illumina, Inc.) at 37˚C for 15 min, followed by incubation at 85˚C for 3 min. The RNase R was used at a concentration of 3 U/$\mu$g RNA. RNA samples were subjected to reverse transcription using the GoScript™ Reverse Transcription System (cat. no. A5001; Promega Corporation) under the following optimized conditions: Initial primer annealing step at 25˚C for 5 min, followed by cDNA synthesis

at 42˚C for 45 min, and final enzyme inactivation at 70˚C for 15 min. The expression of circEFR3A was subsequently detected using reverse transcription-quantitative polymerase chain reaction (RT-qPCR).

*RT-qPCR, nucleic acid agarose gel electrophoresis, and Sanger sequencing*. cDNA was synthesized from total RNA using the GoScript™ Reverse Transcription System Kit (Promega Corporation), following the manufacturer's standard protocol. qPCR reaction was then performed using the GoTaq® qPCR Master Mix (Promega Corporation) on an Applied Biosystems fluorescence quantitative PCR instrument (Thermo Fisher Scientific, Inc.). The thermocycling conditions included an initial denaturation at 95˚C for 5 min, followed by 40 cycles of denaturation at 95˚C for 15 sec, annealing at 58˚C for 30 sec, and extension at 72˚C for 30 sec, with a final extension at 72˚C for 10 min. circEFR3A and miR-590-3p levels were quantified using specific primers (Guangzhou RiboBio Co., Ltd.). All primer sequences used for PCR amplification are listed in Table SI. Relative expression levels were determined using the $2^{-\Delta\Delta Cq}$ method (21). For RT-PCR, the reaction was prepared using GoTaq Green Master Mix (cat. no. M712B; Promega Corporation) and PCR was performed using a ProFlex PCR System (Thermo Fisher Scientific, Inc.) with the following thermocycling protocol: Initial denaturation at 95˚C for 2 min; followed by 25-35 cycles of 95˚C for 30 sec, 60˚C for 30 sec and 72˚C for 1 min/kb (product length); with a final extension at 72˚C for 5 min. The PCR products were then separated by 2% agarose gel electrophoresis, and the band intensity was detected using ultraviolet irradiation. Following confirmation of specific amplification using gel agarose electrophoresis, the PCR products were purified using the Agarose Gel DNA Extraction Kit (cat. no. DP209; Tiangen Biotech Co., Ltd.). Finally, the nucleotide sequence of the PCR products was determined using Sanger sequencing analysis (Sangon Biotech Co., Ltd.). The primers used are listed in Table SI.

*Cell Counting Kit-8 (CCK-8) assay*. For the CCK-8 assay, pre-treated MDA-MB231 and MDA-MB-453 cells (experimental group) and untreated cells (control group) were seeded into 96-well plates at a density of 3,000 cells/well. Following cell adherence, cell viability was assessed using the CCK-8 reagent (cat. no. SC119-01; Seven Innovations (Beijing) Biotechnology Co., Ltd.) at 0, 24, 48, 72 and 96 h post-seeding. The procedure involved adding 10 $\mu$l CCK-8 reagent to each well. After briefly shaking the plate to mix, the cells were incubated at 37˚C for 2 h. The absorbance at 450 nm was subsequently measured using a microplate reader (Tecan Group, Ltd.).

*Colony formation assay*. MDA-MB231 and MDA-MB-453 cells from both the experimental and control groups were seeded at a density of 1,000 cells/well in a 6-well plate and incubated at 37˚C for ~10 days until visible cell colonies formed. The colonies were fixed with 4% paraformaldehyde for 20 min at room temperature and stained with 0.1% crystal violet for 20 min at room temperature. After which, images of the colonies (defined as >60 cells) in each well were captured and counted under a light microscope (EVOS XL Core Cell Imaging System; Thermo Fisher Scientific, Inc.). Quantification was performed using ImageJ software (v1.53; National Institutes of Health).

*Transwell assay*. Transwell migration and invasion assays were performed using an uncoated chamber for migration and a Matrigel-coated chamber for invasion, as per the manufacturer's instructions (BD Biosciences). For the invasion assay, 60 $\mu$l Matrigel (1:8 in serum-free medium) was polymerized at 37˚C for 2 h to establish a uniform basement membrane matrix. MDA-MB231 and MDA-MB-453 cells from both groups were seeded into the upper chamber of 24-well plates at a density of $2x10^5$ cells/well. The upper compartment of the 24-well Transwell chamber contained 200 $\mu$l RPMI-1640 (without serum), whereas the lower compartment contained 600 $\mu$l complete medium. The plates were incubated at 37˚C for 48 h. Following incubation, cells were fixed with 1 ml 4% paraformaldehyde solution for 20 min at room temperature. Finally, the fixed cells were stained with 0.1% crystal violet for 10 min at room temperature, and counted across ≥3 randomly selected fields using the EVOS XL Core Cell Imaging System to quantify migration and invasion.

*Fluorescence in situ hybridization (FISH)*. The biotin-labeled circEFR3A probe was purchased from Guangzhou RiboBio Co., Ltd and the FITC-labeled miR-590-3p probe was purchased from Guangzhou Geneseed Biotech, Co., Ltd. (5'FITC-ACTAGCTTATACATAAAATTA-3'FITC). For cell-based FISH, MDA-MB-231 and MDA-MB-453 cells were cultured on coverslips overnight and then fixed with 4% paraformaldehyde for 20 min at room temperature. After prehybridization in PBS containing 0.5% Triton X-100, cells were hybridized in hybridization buffer (Guangzhou Geneseed Biotech, Co., Ltd.) (40% formamide, 10% Dextran sulfate, 1X Denhardt's solution, 4X SSC, 10 mM DDT, 1 mg/ml yeast transfer RNA, 1 mg/ml sheared salmon sperm DNA) with the circEFR3A and miR-590-3p probes (diluted to a concentration of 20 nM) at 37˚C overnight. For tissue-based FISH, the tissues were fixed in 10% neutral buffered formalin at room temperature for 24-48 h embedded in paraffin- and cut into 5-$\mu$m sections, after which, the tissues were assessed following standard protocols. Tissue sections were sequentially deparaffinized in xylene (3x5 min), rehydrated through a graded ethanol series (50, 75, 85 and 95%; 2 min each), and subjected to protein digestion with 50 $\mu$l Proteinase K solution (15 $\mu$g/ml in TE buffer, pH 8.0) at 37˚C for 30 min, followed by three washes in nuclease-free distilled water. Pre-hybridization and circEFR3A hybridization procedures followed the previously described method. Nuclei were stained with DAPI for 10 min at 37˚C, and signals were observed using an LSM 900 confocal microscope (Zeiss GmbH).

*Luciferase reporter assay*. Wild-type and mutant circEFR3A constructs were obtained from Guangzhou Geneseed Biotech, Co., Ltd. To further assess the interaction between AR and miR-590-3p, psiCHECK2 vectors containing the wild-type and mutant 3'UTR sequences of AR were purchased from Guangzhou Geneseed Biotech, Co., Ltd. MDA-MB231 and MDA-MB-453 cells were seeded in 12-well plates and incubated overnight at 37˚C for adherence. Subsequently, luciferase assays were performed to measure the activity of

wild-type or mutant luc-circEFR3A vectors co-transfected with miR-NC or miR-590-3p mimics in MDA-MB-231 cells, as well as the activity of wild-type or mutant AR 3'UTR vectors co-transfected with miR-590-3p mimics or a negative control in MDA-MB-453 cells, using Lipofectamine® 3000 transfection reagent (Invitrogen; Thermo Fisher Scientific, Inc.). After 48 h of co-transfection, cell lysates were prepared using the Luciferase Reporter Gene Assay Kit (Promega Corporation), and luciferase activity was measured using a Tecan Spark Multifunctional Microplate Reader (Tecan Group, Ltd.) following the Dual Luciferase Reporter Gene Assay System (Promega Corporation) instructions. Luciferase activity was standardized by comparison with *Renilla* luciferase activity.

*RNA immunoprecipitation (RIP) assay*. MDA-MB-231 cells were co-transfected with a Myc-tagged AGO2 vector (1 $\mu$g; cat. no. RC228592; OriGene Technologies, Inc.) and miR-590-3p mimics (50 nM) using Lipofectamine 3000 transfection reagent according to the manufacturer's protocol. Cells were maintained at 37˚C in a 5% $CO_2$ incubator during the 48-h transfection period, and subsequent experiments were performed 72 h post-transfection. RIP assays were performed using the Magna RIP Kit (MilliporeSigma; Merck KGaA) according to the manufacturer's instructions. Briefly, cells were lysed in RIP lysis buffer supplemented with protease and RNase inhibitors. The lysates were then incubated at room temperature for 1 h with magnetic beads conjugated to either anti-Myc antibody (cat. no. ab9132; Abcam; 5 $\mu$g per RIP reaction) or anti-IgG control antibody (cat. no. ab172730; Abcam; 5 $\mu$g per RIP reaction). Immunoprecipitation was performed by incubating the antibody-bound beads with the cell lysates overnight at 4˚C. Following purification of the immunoprecipitated RNA, the levels of circEFR3A were quantified using RT-qPCR. The RT-qPCR method was the same as aforementioned, and the primers are listed in Table SI.

*Western blotting*. Western blotting was performed according to standard protocol. Following transfection, MDA-MB-453 cells were incubated for 48 h and total protein was extracted using RIPA lysis buffer (Invitrogen; Thermo Fisher Scientific, Inc.). Protein concentrations were quantified using the BCA assay (Thermo Fisher Scientific, Inc.). Equal amounts of protein lysates (40 $\mu$g/lane) were separated by 10% SDS-polyacrylamide gel electrophoresis and subsequently transferred to polyvinylidene fluoride membranes (MilliporeSigma; Merck KGaA), which were blocked with 5% skimmed milk in PBS-0.1% Tween-20 at room temperature for 1.5 h. The membranes were then incubated with the following antibodies at 4˚C overnight: Rabbit polyclonal anti-AR (1:1,000; cat. no. 22089-1-AP; Proteintech Group, Inc.) and anti-β-actin (1:1,000; cat. no. 20536-1-AP; Proteintech Group, Inc.). Proteins were then incubated for 1 h at room temperature with HRP-conjugated goat anti-rabbit IgG H&L secondary antibody (1:2,000; cat. no. ab6721; Abcam). Protein bands were visualized using an enhanced chemiluminescence detection system (Beijing Solarbio Science Technology, Co., Ltd.) following the manufacturer's instructions. β-actin served as a loading control.

*Bioinformatics analysis*. The Gene Expression Profiling Interactive Analysis (GEPIA) database (v2.0; http://gepia.cancer-pku.cn/) was used to evaluate the expression level of AR in BC tissue, applying a significance cutoff of |log2FC| >1 and adjusted P-value (q-value) <0.05. Targetscan (v7.2; https://www.targetscan.org/mamm_31/) and Miranda (v3.3a; http://www.microrna.org/microrna/home.do) were used to predict the potential binding miRNA for circEFR3A. Additionally, target gene prediction for miR-590-3p was performed using Genecards (v5.12; https://www.genecards.org/), Targetscan and miRPathDB (v2.0; https://mpd.bioinf.uni-sb.de/mirna.html?mirna). RNA secondary structure predictions were performed using the RNAfold web server (version 2.6.3; http://rna.tbi.univie.ac.at/cgi-bin/RNAWebSuite/RNAfold.cgi). Differentially expressed mRNA-enriched pathways of miR-590-3p were identified using Reactome pathway analysis in the miRPathDB database (version 2.0; https://mpd.bioinf.uni-sb.de/), following the guidelines of the databases.

*Statistical analysis*. Statistical significance for all experiments was assessed using SPSS 23.0 software (IBM Corp.). For numerical data, either unpaired Student's t-test or one-way ANOVA followed by Tukey's post hoc test were used for statistical analysis. By contrast, categorical data were assessed using the $\chi^2$ test. The correlation between circEFR3A and AR was analyzed by Pearson's correlation analysis. All statistical tests performed were two-sided, and $P<0.05$ was considered to indicate a statistically significant difference.

## Results

*Characterization of circEFR3A in BC cells*. The circRNA, circEFR3A, designated as hsa_circ_0006522 in the circBase database, derives its name from its origin in the EFR3A gene located on chromosome 8. To assess the circular structure of circEFR3A, both divergent and convergent primers were designed. PCR amplification was performed using two distinct templates: cDNA synthesized by reverse transcription and genomic DNA extracted from the BC cell line MDA-MB-231. The experiments demonstrated that divergent primers specifically amplified the circular form of EFR3A in cDNA, whilst convergent primers amplified the linear form in both cDNA and genomic DNA samples (Fig. 1A). These findings indicate that circEFR3A exists as a circRNA molecule in BC cells. Moreover, the junction sequence of circEFR3A was confirmed through Sanger sequencing (Fig. 1A).

To evaluate the biological role of circEFR3A in BC cells, its expression was assessed in multiple BC cell lines (MDA-MB-231, SK-BR-3, MCF7, BT-549 and MDA-MB-453) using RT-qPCR, revealing the highest expression in MDA-MB-231 cells and the lowest in MDA-MB-453 cells (Fig. 1B). After treating MDA-MB-231 and MDA-MB-453 cells with Actinomycin D, the relative expression of circEFR3A and linearEFR3A mRNA was indicated over time using RT-qPCR (Fig. 1C). Further stability testing using RNase R treatment on total RNA from MDA-MB-231 and MDA-MB-453 cells demonstrated that circEFR3A was resistant to RNase R digestion, unlike linear EFR3A, which decreased post-treatment (Fig. 1D). FISH assay results also demonstrated that circEFR3A was primarily located in the cytoplasm of MDA-MB-231 and MDA-MB-453 cells (Fig. 1E).

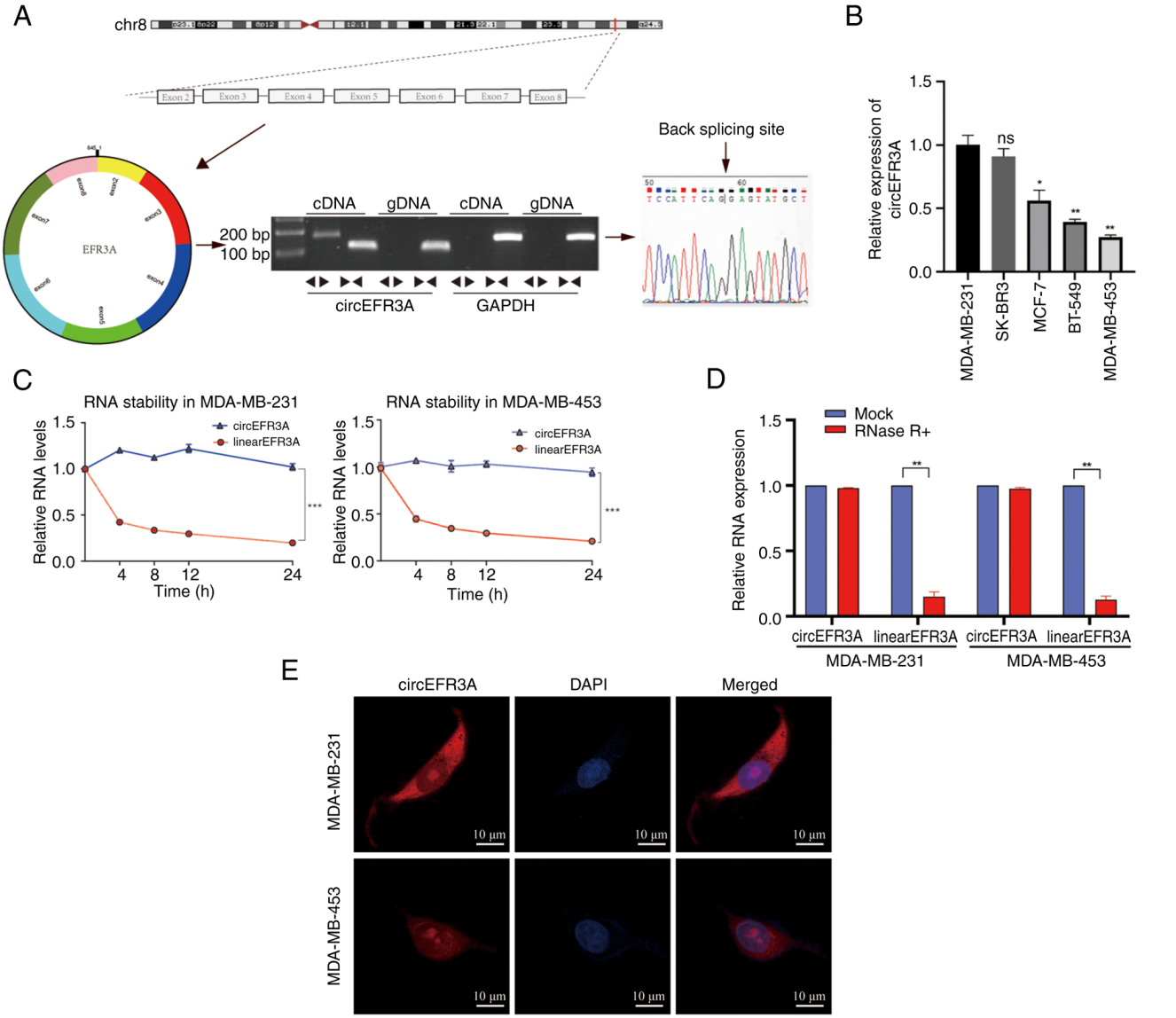


Figure 1. Characterization of circEFR3A in breast cancer cells. (A) Splicing site sequence and circularization schematic of circEFR3A. Divergent primers successfully amplified the circular RNA transcript circEFR3A in cDNA but not in gDNA. By contrast, convergent primers amplified the linear RNA transcript circEFR3A in both cDNA and gDNA. GAPDH served as an internal control. (B) Expression level of circEFR3A in SK-BR-3, MCF7, BT-549 and MDA-MB-453 cells compared with MDA-MB-231 cells. (C) Relative expression levels of circEFR3A and linear EFR3A mRNA were assessed using RT-qPCR following Actinomycin treatment in MDA-MB-231 and MDA-MB-453 cells at the indicated time points. (D) mRNA expression of circEFR3A and linear EFR3A in RNase R-treated breast cancer cells, assessed using RT-qPCR. (E) Subcellular localization of circEFR3A was determined using fluorescence *in situ* hybridization. Scale bar, 10 $\mu$m. $^{*}$P<0.05; $^{**}$P<0.01; $^{***}$P<0.001 vs. MDA-MB-231 cells or as indicated. Circ, circular; cDNA, complementary DNA; gDNA, genomic DNA; RT-qPCR, reverse transcription-quantitative PCR; ns, not significant; bp, base pairs.

*circEFR3A is associated with BC progression and promotes BC cell proliferation, migration and invasion*. The expression level of circEFR3A in BC specimens was initially assessed using FISH. Tissue microarrays were purchased and a total of 129 BC tissues were assessed, categorized into low- and high-expression groups based on the following criteria: i) Score 0, no red fluorescence or weak expression in the majority of cells; ii) score 1, moderate expression in most cells or medium intensity expression in >50% of cells; and iii) score 2, moderate or high intensity expression in the majority of cells. A score of ≤1 was defined as low expression, whilst a score of >1 was defined as high expression. All 129 BC tissue samples were obtained from female patients. The clinicopathological characteristics of these patients and their corresponding circEFR3A expression levels are presented in Table I. Analysis of these data revealed no statistically significant differences in circEFR3A expression across several parameters, including age, histological grades and clinical stages. Similarly, no significant associations were observed between circEFR3A expression, tumor size, lymph node metastasis status or the expression of estrogen receptor, progesterone receptor and human epidermal growth factor receptor 2.

To assess the prognostic significance of circEFR3A, the Kaplan-Meier method was used to analyze its impact on patient outcomes in the 129 BC tissue samples. Analysis revealed a statistically significant difference in overall survival (OS) between patients with high and low expression levels, with

Table I. Association between clinicopathological characteristics and circEFR3A expression in patients with breast cancer (n=129).

| Clinicopathological characteristic | n | circEFR3A expression | | P-value | $\chi^2$ |
|---|---|---|---|---|---|
| | | Low | High | | |
| Age | | | | 0.561 | 0.338 |
| ≤50 years | 59 | 17 | 42 | | |
| >50 years | 70 | 17 | 53 | | |
| Histological grade | | | | 0.469 | 0.525 |
| G1 | 32 | 10 | 22 | | |
| G2-3 | 97 | 24 | 73 | | |
| TNM stage | | | | 0.230 | 1.440 |
| I-II | 83 | 19 | 64 | | |
| III | 46 | 15 | 31 | | |
| Tumor invasion | | | | 0.699 | 0.718 |
| T1 | 27 | 7 | 20 | | |
| T2 | 88 | 22 | 66 | | |
| T3 | 14 | 5 | 9 | | |
| Lymph node metastasis | | | | 0.705 | 1.403 |
| N0 | 47 | 11 | 36 | | |
| N1 | 39 | 9 | 30 | | |
| N2 | 35 | 11 | 24 | | |
| N3 | 8 | 3 | 5 | | |
| HER2 | | | | 0.055 | 3.697 |
| Positive | 33 | 4 | 29 | | |
| Negative | 96 | 30 | 66 | | |
| ER | | | | 0.865 | 0.029 |
| Positive | 85 | 22 | 63 | | |
| Negative | 44 | 12 | 32 | | |
| PR | | | | 0.857 | 0.033 |
| Positive | 70 | 18 | 52 | | |
| Negative | 59 | 16 | 43 | | |
| Molecular type | | | | 0.892 | 0.229 |
| Luminal A/B type | 85 | 22 | 63 | | |
| HER-2 positive type | 17 | 4 | 13 | | |
| Triple negative type | 27 | 8 | 19 | | |

TNM, tumor-node-metastasis; G, grade; T, tumor; N, lymph node; HER2, human epidermal growth factor receptor 2; ER, estrogen receptor; PR, progesterone receptor.

the high-expression group exhibiting significantly reduced OS (Fig. 2A and B).

To further elucidate the factors influencing the prognosis of patients with BC, univariate analysis was performed on the survival data, followed by multivariate Cox regression analysis on factors exhibiting statistical significance (Table II). The findings indicated that circEFR3A expression [hazard ratio (HR), 3.959; P=0.005], clinical stage (HR, 2.709; P=0.002) and the triple negative molecular type (HR, 2.923; P=0.003) serve as independent prognostic factors for patients with BC.

For functional analysis, circEFR3A siRNA targeting its junction site was transfected into MDA-MB-231 cells. RT-qPCR confirmed circEFR3A knockdown compared with the si-NC (Fig. 2C). CCK-8 assays revealed that si-circEFR3A transfection significantly reduced MDA-MB-231 cell proliferation (Fig. 2D), and colony formation assays demonstrated significantly reduced colony formation in si-circEFR3A transfected cells (Fig. 2E), compared with the controls. Additionally, Transwell assays revealed that MDA-MB-231 cells treated with si-circEFR3A exhibited significantly reduced rates of migration and invasion (Fig. 2F). By contrast, transfection of MDA-MB-453 cells was performed using a circEFR3A overexpression plasmid; RT-qPCR revealed significantly increased circEFR3A levels post-transfection compared with those in the pLC5-ciR group (Fig. 2G). Moreover, CCK-8 and colony formation assays demonstrated significantly increased rates of proliferation in circEFR3A-overexpressing MDA-MB-453 cells compared with those in the pLC5-ciR

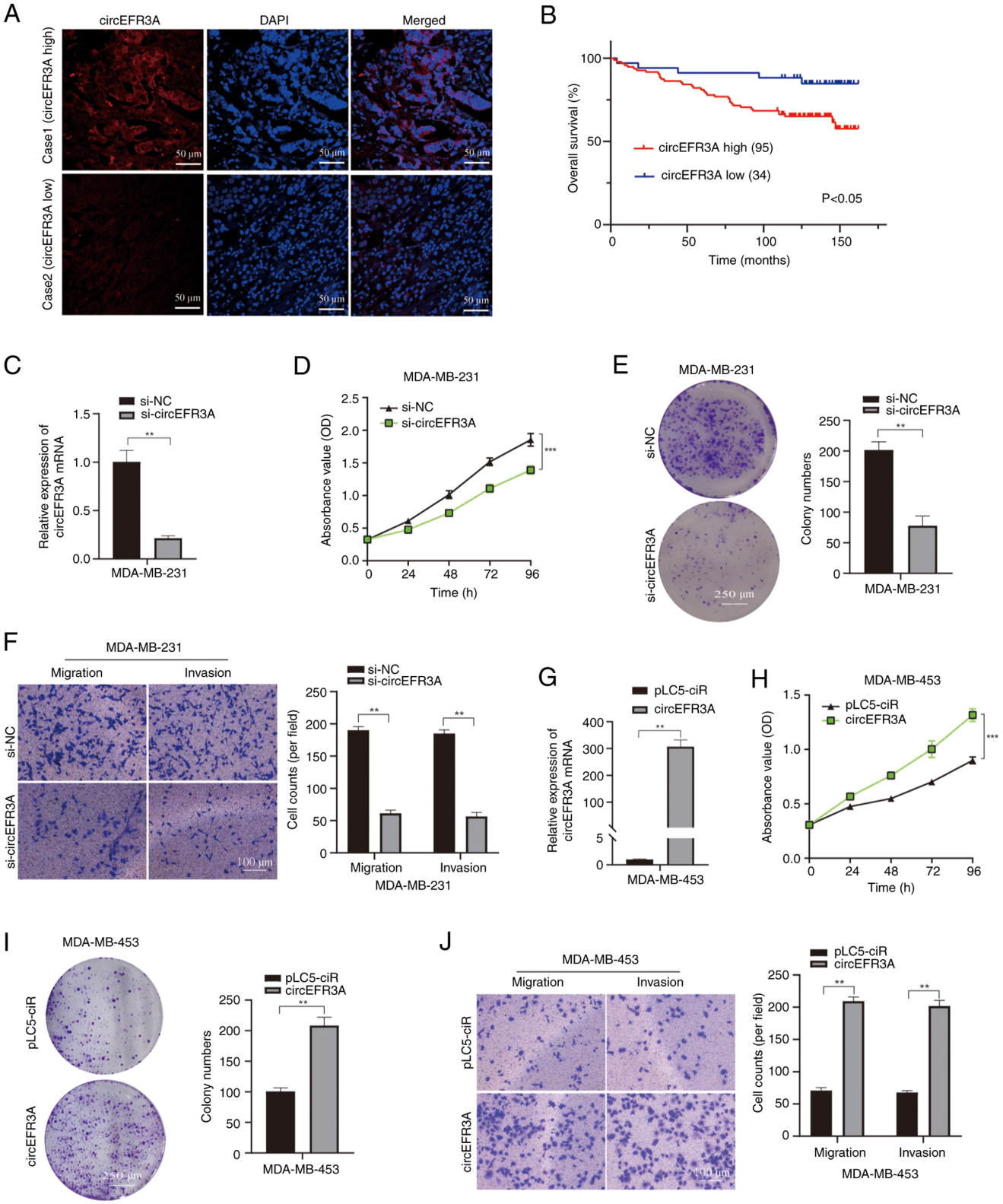


Figure 2. circEFR3A is associated with breast cancer progression and promotes breast cancer cell proliferation, migration and invasion. (A) Fluorescence *in situ* hybridization analysis revealed the expression level of circEFR3A in breast cancer tissue specimens. Scale bar, 50 $\mu$m. (B) Survival analysis demonstrated that patients with breast cancer with high circEFR3A expression had a worse prognosis compared with those with low expression. (C) Quantification of circEFR3A Levels in MDA-MB-231 cells following transfection with circEFR3A siRNA. (D) CCK-8 assay results demonstrated that reduced circEFR3A expression significantly inhibited the proliferation of MDA-MB-231 cells. (E) Colony formation assay results revealed a significant reduction in the number of cell colonies following circEFR3A knockdown in breast cancer cells. Scale bar, 250 $\mu$m. (F) Transwell assay results indicated that knockdown of circEFR3A expression suppressed migration and invasion in MDA-MB-231 cells. Scale bar, 100 $\mu$m. (G) Level of circEFR3A in MDA-MB-453 cells after transfection with circEFR3A, assessed using reverse transcription-quantitative PCR. (H) CCK-8 assay results demonstrated that circEFR3A overexpression significantly enhanced the proliferation of MDA-MB-453 cells. (I) Colony formation assay results indicated a significant increase in the number of cell colonies following circEFR3A overexpression in MDA-MB-453 cells. Scale bar, 250 $\mu$m. (J) Transwell assay results demonstrated that circEFR3A overexpression promoted the migration and invasion of MDA-MB-453 cells. Scale bar, 100 $\mu$m. $^{**}$P<0.01; $^{***}$P<0.001. Circ, circular; si, small interfering; CCK-8, Cell Counting Kit-8; OS, overall survival; NC, negative control; OD, optical density.

Table II. Univariate and multivariate Cox-regression analysis of prognostic factors for patients with breast cancer (n=129).

| | Univariate analysis | | | Multivariate analysis | | |
|---|---|---|---|---|---|---|
| Prognostic factor | HR | 95% CI | P-value | HR | 95% CI | P-value |
| Age (≤50 vs. >50 years) | 1.262 | 0.670, 2.377 | 0.471 | | | |
| Histological grade (G1 vs. G2-3) | 1.503 | 0.687, 3.285 | 0.308 | | | |
| Clinical stage (I-II vs. III) | 2.155 | 1.159, 4.006 | 0.015[a] | 2.709 | 1.434, 5.120 | 0.002[a] |
| Tumor invasion (T1 vs. T2-3) | 1.335 | 0.591, 3.019 | 0.487 | | | |
| Lymph node metastasis (N0 vs. N1-3) | 1.333 | 0.688, 2.584 | 0.395 | | | |
| ER (Positive vs. negative) | 2.116 | 1.136, 3.940 | 0.018[a] | | | |
| PR (Positive vs. negative) | 1.694 | 0.907, 3.162 | 0.098 | | | |
| HER2 (Positive vs. negative) | 0.955 | 0.466, 1.956 | 0.900 | | | |
| circEFR3A expression (Low vs. high) | 2.976 | 1.164, 7.611 | 0.023[a] | 3.959 | 1.519, 10.320 | 0.005[a] |
| Molecular type | | | | | | |
| Luminal A/B vs. HER-2 positive | 1.612 | 0.650, 3.996 | 0.303 | | | |
| Luminal A/B vs. triple negative | 2.474 | 1.237, 4.950 | 0.010[a] | 2.923 | 1.448, 5.901 | 0.003[a] |

[a]P<0.05. Reference is the first item. ER was not included in the multivariate analysis as it is a linearly associated variable: ER positive vs. ER negative = Luminal A/B vs. HER-2 positive + Triple negative. HR, hazard ratio; CI, confidence interval; G, grade; T, tumor; N, lymph node; HER2, human epidermal growth factor receptor 2; ER, estrogen receptor; PR, progesterone receptor.

group (Fig. 2H and I). Furthermore, Transwell assays indicated that circEFR3A overexpression significantly promoted migration and invasion in MDA-MB-453 cells compared with those in the pLC5-ciR group (Fig. 2J). Collectively, these findings indicate that circEFR3A enhances BC cell proliferation, migration and invasion.

*circEFR3A acts as a miR-590-3p sponge in BC cells*. The aforementioned findings demonstrated that circEFR3A may be abundantly expressed in BC cells and is mainly localized in the cytoplasm, making it possible for circEFR3A to act as a miRNA sponge. The Miranda and TargetScan databases were used to predict the miRNA with the strongest binding affinity to circEFR3A, which was identified as miR-590-3p (Fig. 3A). The RNAfold web server was employed to predict the minimum free energy secondary structure of circEFR3A, as well as to predict two potential binding sites between the secondary structure of circEFR3A and miR-590-3p (Fig. 3B).

To assess the effect of miR-590-3p on the expression of circEFR3A, luciferase-tagged circEFR3A (luc-circEFR3A) and miR-590-3p mimics were co-transfected into the highly expressing circEFR3A MDA-MB-231 cell line and a luciferase reporter assay was performed. Successful transfection of miR-590-3p mimics into MDA-MB-231 cells was confirmed (Fig. S1). The results demonstrated that miR-590-3p significantly inhibited the luciferase activity of luc-circEFR3A compared with miR-NC (Fig. 3C). A RIP assay was also used to evaluate the interaction between circEFR3A and miR-590-3p. The results showed that circEFR3A was significantly enriched in anti-Myc immunoprecipitates compared with anti-IgG controls in MDA-MB-231 cells co-transfected with Myc-AGO2 and miR-590-3p mimics (Fig. 3D). Additionally, knockdown of circEFR3A expression was associated with a significant increase in miR-590-3p expression relative to si-NC controls (Fig. 3E). Finally, the FISH assay results demonstrated that both circEFR3A and miR-590-3p are localized in the cytoplasm and exhibit co-localization (Fig. 3F), suggesting that circEFR3A may act as a sponge for miR-590-3p in BC cells.

*miR-590-3p inhibits the proliferation, migration and invasion of BC cells*. The biological role of miR-590-3p in BC was assessed by introducing a miR-590-3p inhibitor into MDA-MB-231 cells, allowing evaluation of the effects of miR-590-3p downregulation on cellular functions (Fig. 4A). Compared with in the miR-NC group, CCK-8 and colony formation assays demonstrated that decreased miR-590-3p levels significantly promoted MDA-MB-231 cell proliferation (Fig. 4B and C). Additionally, Transwell migration and invasion assays demonstrated that reduced miR-590-3p expression enhanced significantly increased the rates of migration and invasion of MDA-MB-231 cells compared with those in the miR-NC group (Fig. 4D). By contrast, to assess the effects of increased miR-590-3p expression on cellular functions, MDA-MB-453 cells were transfected with miR-590-3p mimics (Fig. 4E). Results from the CCK-8 and colony formation assays indicated a significant decrease in the proliferation rate of MDA-MB-453 cells post-transfection with miR-590-3p mimics compared with that in the miR-NC group (Fig. 4F and G). Transwell experiments also revealed that the transfection with miR-590-3p mimics into MDA-MB-453 cells led to a significant reduction in migration and invasion compared with in the miR-NC group (Fig. 4H). Collectively, these findings suggest that miR-590-3p may inhibit BC cell proliferation, migration and invasion.

*circEFR3A promotes proliferation, migration and invasion in BC via miR-590-3p*. To assess how circEFR3A exerts its promoting functions in BC cells, MDA-MB-453 cells were transfected with either circEFR3A alone or in combination

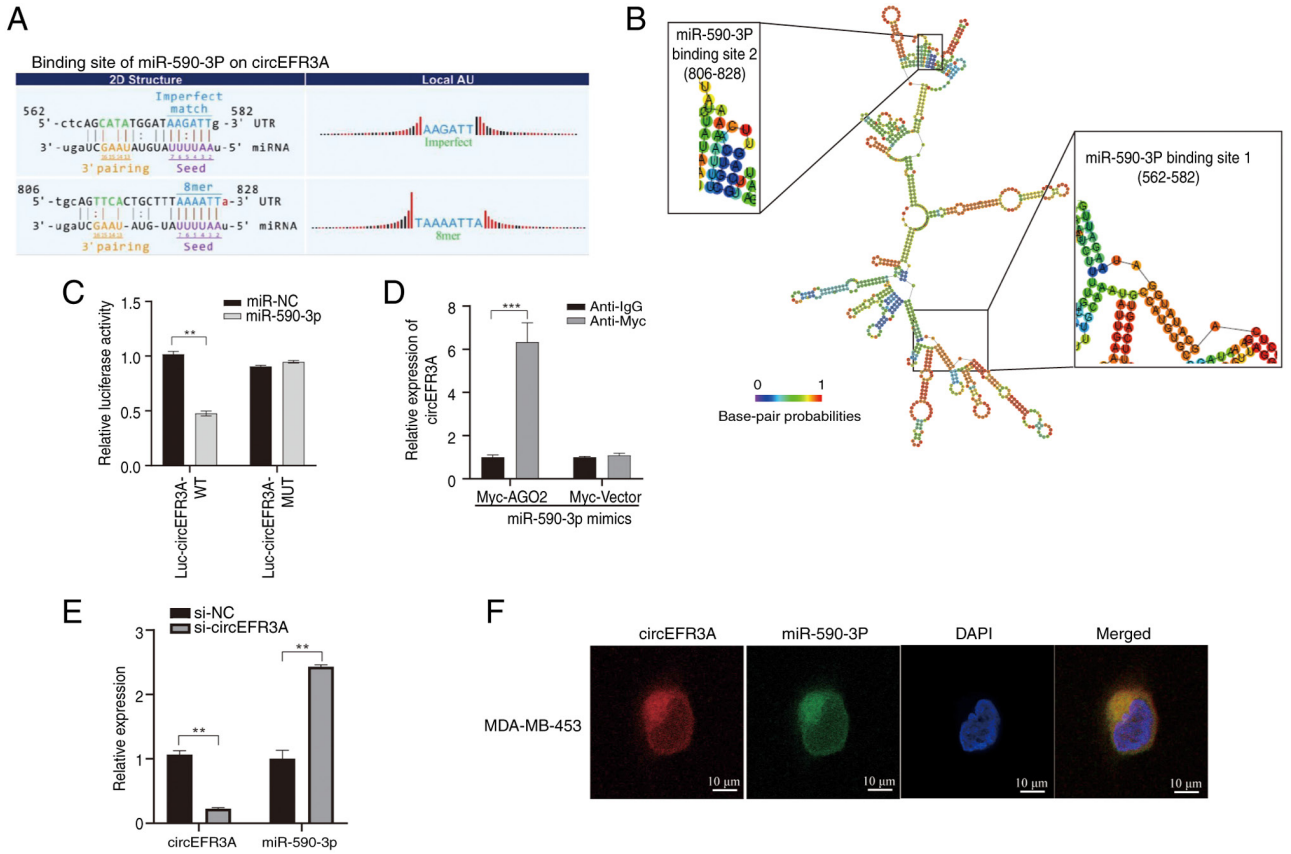


Figure 3. circEFR3A serves as a miR-590-3p sponge in breast cancer cells. (A) Predicting miRNA that bind to circEFR3A based on the TargetScan and miRanda databases. (B) Minimum free energy secondary structure of circEFR3A was predicted using the RNAfold web server, highlighting the regions relevant for miR-590-3p binding. (C) Luciferase assay was performed to determine the luciferase activity of circEFR3A when co-transfected with wild-type or mutant luc-circEFR3A vector and miR-NC or miR-590-3p mimics in MDA-MB-231 cells. (D) RIP assay was performed to assess the binding between circEFR3A and miR-590-3p, confirming their interaction. Experiments were repeated three times. (E) MDA-MB-231 cells were transfected with si-NC or si-circEFR3A, followed by reverse transcription-quantitative PCR to assess the relative expression levels of circEFR3A and miR-590-3p. (F) Fluorescence *in situ* hybridization demonstrated that circEFR3A and miR-590-3p were co-localized in the cytoplasm of MDA-MB-453 cells. Scale bar, 10 $\mu$m. $^{**}$P<0.01; $^{***}$P<0.001. Circ, circular; miR/miRNA, microRNA; NC, negative control; RIP, RNA immunoprecipitation; si, small interfering.

with miR-590-3p mimics. Compared with in the pLC5-ciR + miR-NC group, CCK-8 and colony formation assays demonstrated that circEFR3A overexpression alone significantly increased the proliferation of MDA-MB-453 cells. However, the introduction of miR-590-3p mimics counteracted this effect (Fig. 5A and B); Furthermore, whilst circEFR3A overexpression significantly increased the rates of migration and invasion of MDA-MB-453 cells, simultaneous transfection with miR-590-3p mimics reversed these increases (Fig. 5C and D). Compared with in the pLC5-ciR + miR-NC group, *in vivo* experiments using nude mice revealed that circEFR3A overexpression significantly promoted xenograft tumor growth; however, this promotional effect was reversed transfection with miR-590-3p (Fig. 5E-H). These findings indicate that circEFR3A promotes BC cell proliferation, migration and invasion, at least in part, by modulating miR-590-3p activity.

*circEFR3A restores miR-590-3p mediated targeted repression of the oncogene AR in BC cells*. To elucidate the molecular mechanism of miR-590-3p in BC, three commonly used online databases were utilized: Targetscan, miRPathDB and Genecards. Targetscan and miRPathDB are widely used online tools for predicting miRNA target genes. Their basic principle is based on the binding of the miRNA seed sequence to the 3' UTR of the target gene mRNA. The tightness and specificity of this binding determine the regulatory effect of the miRNA on the target gene. The GeneCards database collects genes closely associated with the occurrence and development of BC (22,23). Taking the intersection of these databases can further filter out genes closely related to BC progression that are targeted by miR-590-3p. This comprehensive methodology enabled the identification of potential miR-590-3p target genes pertinent to BC development. miRPathDB was used to forecast the downstream signaling pathways influenced by miR-590-3p. The Reactome pathway analysis, a function within miRPathDB, revealed significant enrichment of miR-590-3p in the cancer-associated post-translational protein modification pathway (Fig. 6A). Subsequently, potential target genes of miR-590-3p were identified using the Targetscan and miRPathDB databases, intersecting these targets with key BC genes from the Genecards database, along with genes enriched in the post-translational modification pathway. This analysis pinpointed AR as a likely downstream target of miR-590-3p (Fig. 6B).

Moreover, the binding site of miR-590-3p in the AR 3'UTR was predicted, and wild-type or mutant AR 3'UTR luciferase reporter vectors were constructed (Fig. 6C). MDA-MB-453 cells were co-transfected with AR 3'UTR constructs (either

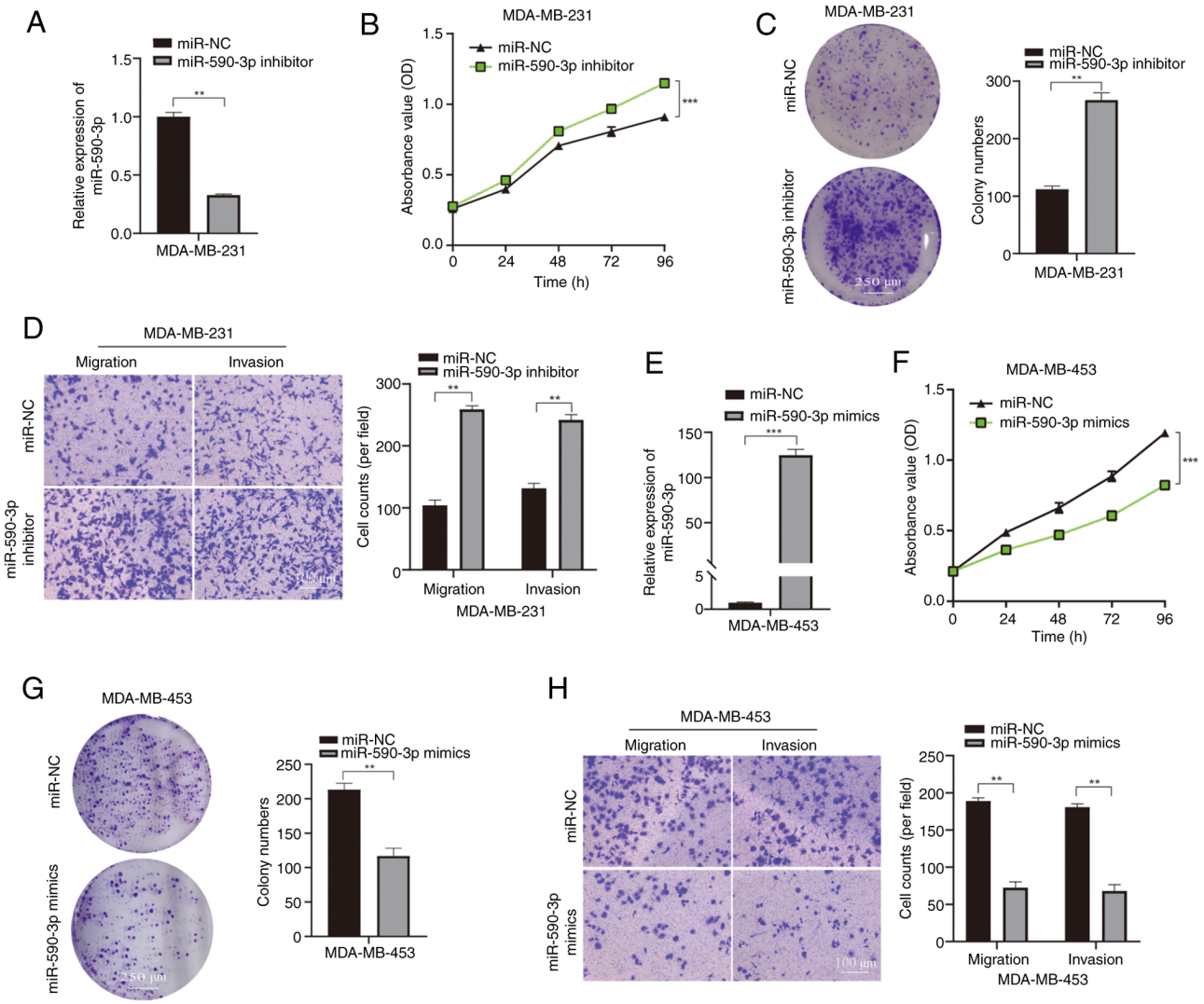


Figure 4. miR-590-3p inhibits the proliferation, migration and invasion of breast cancer cells. (A) Expression levels of miR-590-3p in MDA-MB-231 cells, assessed using RT-qPCR. (B) CCK-8 assay results revealed that miR-590-3p low expression significantly enhanced the proliferation of MDA-MB-231 cells. (C) Colony formation assay results revealed a significant increase in the number of cell colonies following miR-590-3p downregulation in MDA-MB-231 cells. Scale bar, 250 $\mu$m. (D) Transwell assay results demonstrated that low miR-590-3p expression was significantly associated with an increase in the migration and invasion of MDA-MB-231 cells. Scale bar, 100 $\mu$m. (E) Expression of miR-590-3p in MDA-MB-453 cells, assessed using RT-qPCR. (F) CCK-8 assays revealed that miR-590-3p overexpression significantly promoted the proliferation of MDA-MB-453 cells. (G) Colony formation assay results indicated a significant increase in cell colony formation after miR-590-3p upregulation in MDA-MB-453 cells. Scale bar, 250 $\mu$m. (H) Transwell assay analysis indicated that miR-590-3p overexpression reduced the migration and invasion of MDA-MB-453 cells. Scale bar, 100 $\mu$m. $^{**}$P<0.01; $^{***}$P<0.001. miR, microRNA; RT-qPCR, reverse transcription-quantitative PCR; CCK-8, Cell Counting Kit-8; NC, negative control; OD, optical density.

wild-type or mutant) and miRNA molecules (either miR-NC or miR-590-3p mimics). Subsequently, luciferase reporter assays were performed to assess their interaction. The results demonstrated that compared with in the miR-NC group, co-transfection with miR-590-3P and the wild-type AR 3'UTR vector resulted in a significant reduction in luciferase activity, whereas no significant change was observed for the mutant vector co-transfection group (Fig. 6D), confirming AR as a direct target of miR-590-3p.

The GEPIA database was then used to assess the expression of AR in BC. The results demonstrated that AR expression in 1,085 BC samples was significantly higher than that in 291 normal breast tissue samples (Fig. 6E). At the animal level, three groups of mice were established. Each group received subcutaneous injections of MDA-MB-453 cells that had been stably transfected with one of the following combinations: i) pLC5-ciR + miR-NC; ii) circEFR3A + miR-NC; or iii) circEFR3A + miR-590-3p. The mRNA expression levels of AR were measured in tissues from the three groups of nude mice (n=4/group). The results indicated that, compared with the NC, AR expression was markedly overexpressed in the circEFR3A + miR-NC group. However, this overexpression was reversed with the co-transfection of miR-590-3p (Fig. 6F).

Finally, AR protein expression was evaluated using western blot analysis in MDA-MB-453 cells following transfection with miR-590-3p mimics, with or without the circEFR3A overexpression plasmid. The findings demonstrated that miR-590-3p overexpression markedly downregulated AR protein levels, and circEFR3A counteracted the inhibitory effect of miR-590-3p on AR protein expression (Fig. 6G and H). Correlation analysis also revealed a significant positive correlation between circEFR3A and AR expression levels (Fig. S2).

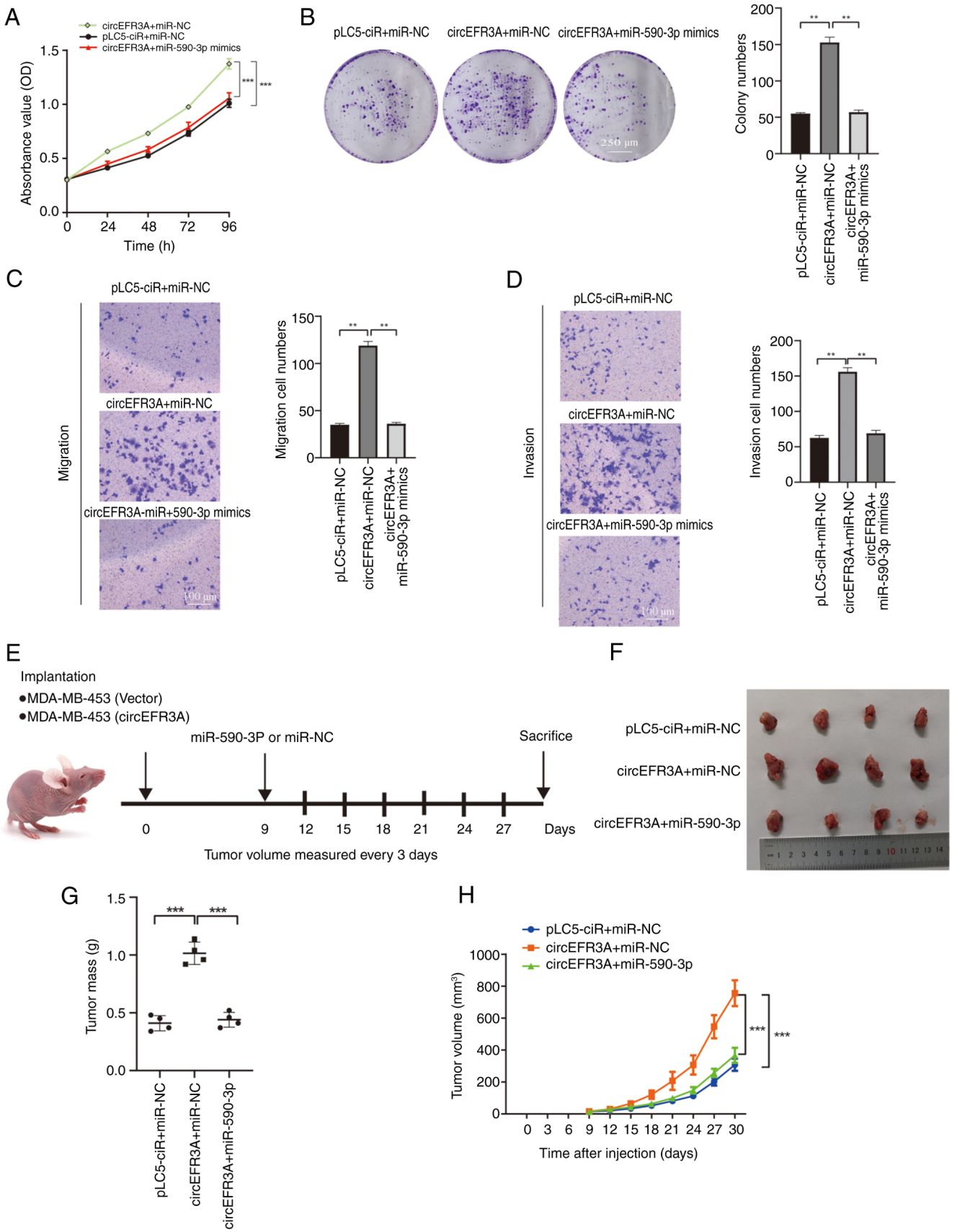


Figure 5. circEFR3A promotes the proliferation, migration and invasion of breast cancer via miR-590-3p. (A) Cell Counting Kit-8 and (B) colony formation assays demonstrated that transfection with circEFR3A alone significantly enhanced the proliferation of MDA-MB-453 cells. Additionally, the pro-proliferative effects of circEFR3A were partially reversed by miR-590-3p mimics. Transwell assay results indicated that transfection with circEFR3A alone significantly increased the (C) migration and (D) invasion rates of MDA-MB-453 cells. However, co-transfection with miR-590-3p mimics partially counteracted these enhanced effects. Scale bar, 100 $\mu$m. (E) Schematic diagram of grouping for the xenotransplantation model. (F) In the xenograft tumor experiment, mice were injected with MDA-MB-453 cells stably transfected with either pLC5-ciR + miR-NC, circEFR3A + miR-NC or circEFR3A + miR-590-3p. (G) Tumor mass and (H) volume were evaluated. $^{**}$P<0.01; $^{***}$P<0.001. circ, circular; miR, microRNA; NC, negative control.

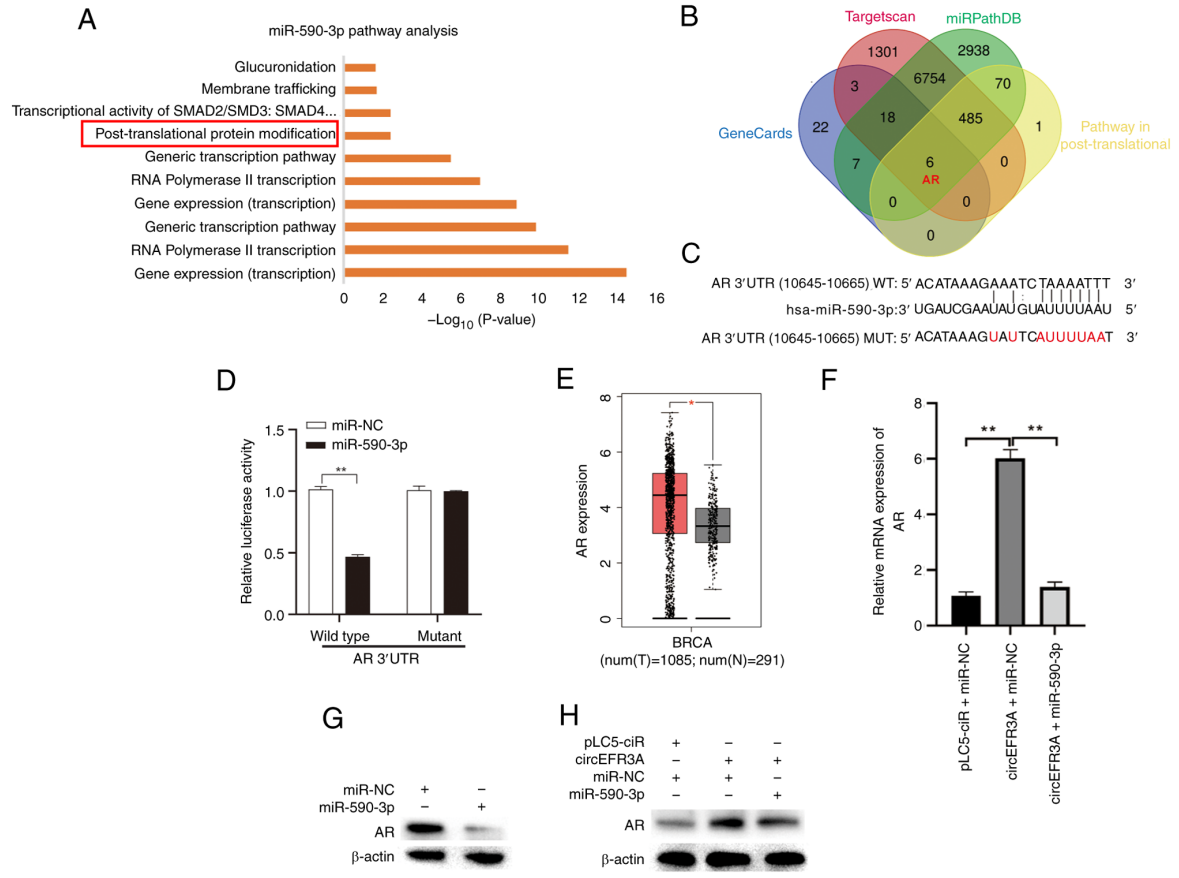


Figure 6. AR is a target gene of miR-590-3p. (A) Downstream signaling pathway of miR-590-3p, predicted using the miRPathDB database. (B) Potential target genes of miR-590-3p, identified using the Targetscan and miRPathDB databases, cross-referenced with key breast cancer genes from the GeneCards database and genes involved in the post-translational protein modification pathway, with intersecting genes visualized in a Venn diagram. (C) Predicted miR-590-3p binding site in AR 3'UTR, along with a diagrammatic depiction of the AR 3'UTR wild-type or mutant reporter constructs. (D) A luciferase reporter assay was performed to measure the activity of the wild-type or mutant AR 3'UTR vector in MDA-MB-453 cells that were co-transfected with either miR-590-3p mimics or a negative control vector. (E) Expression of AR mRNA in 1,085 breast cancer specimens and 291 normal specimens, determined based on the Gene Expression Profiling Interactive Analysis database. (F) Mice were injected with MDA-MB-453 cells stably transfected with either pLC5-ciR + miR-NC, circEFR3A + miR-NC or circEFR3A + miR-590-3p. The mRNA expression levels of AR were measured in tissues from three groups of nude mice. $^{*}$P<0.05; $^{**}$P<0.01. AR protein expression in MDA-MB-453 cells transfected with (G) miR-590-3p or miR-NC and (H) miR-NC or miR-590-3p + circEFR3A or pLC5-ciR+miR-NC was assessed using western blotting. AR, androgen receptor; miR, microRNA; circ, circular; NC, negative control.

These findings indicate that circEFR3A serves as a ceRNA, effectively sponging miR-590-3p and thus rescuing AR from miR-590-3p-induced suppression in BC cells.

## Discussion

CircRNA was first discovered in plants in 1976; however, it was initially considered a byproduct of erroneous splicing. It was not until 2013, when a pivotal study highlighted that circRNAs are a class of ncRNAs with regulatory functions, that circRNAs emerged as a key focus for RNA research (24,25). Over the previous two decades, advancements in high-throughput RNA-sequencing technologies have enabled the identification of specific circRNAs, which are now increasingly acknowledged for their important roles in several diseases (24).

Most circRNAs are formed through a specialized back-splicing process, typically derived from exonic regions of precursor mRNAs, and are primarily localized in the cytoplasm of eukaryotic cells (26). The circular structure of circEFR3A endows it with unique stability. Compared with linear RNA, circEFR3A lacks free 5' and 3' ends, rendering it more resistant to exonucleases. Actinomycin D and RNase R experiments further demonstrate that circEFR3A is more stable than its linear counterpart. This stability ensures a relatively stable intracellular concentration of circEFR3A, providing a foundation for the stable manifestation of its functions (5). Due to their stability, specificity and high expression levels, circRNAs are considered useful biomarkers for several diseases, including for cancer diagnosis and prognosis assessment (27).

The present study identified circEFR3A, which is derived from exons 2-8 of EFR3A pre-mRNA and located on human chromosome 8. Certain studies have reported that EFR3A encodes a protein that is involved in the recruitment of PI4KA kinase to the plasma membrane and thus involved in phosphoinositide metabolism and signaling (28). Mutations in the EFR3A gene have been suggested to be associated with autism and neurological disorders (29,30). However, previous findings suggest that the oncogene KRAS relies on the EFR3A-PI4KA signaling axis to exert oncogenic activity (31). Tissue microarray analysis revealed that high circEFR3A expression was associated with poor prognosis in patients with BC compared with low expression groups. These results indicate that

circEFR3A may serve a role in BC, potentially acting as a biomarker to inform therapeutic strategies for BC.

To date, it has been established that circRNAs influence biological processes through diverse mechanisms, including functioning as miRNA sponges, protein scaffolds and transcription factors, as well as interacting with RNA-binding proteins and encoding polypeptides or proteins (7-10). Among these, the role of circRNAs as miRNA sponges, particularly those derived from exons, has been the most extensively investigated. As circEFR3A is generated through exon circularization and predominantly resides in the cytoplasm, we hypothesized that it may serve as a miRNA sponge. Therefore, the present study aimed to explore this potential function of circEFR3A in BC cells. Miranda and TargetScan databases were used to predict potential miRNAs that could interact with circEFR3A. This screening process led to the identification of miR-590-3p as a candidate. To substantiate the aforementioned hypothesis, a series of experiments were performed, including FISH, RIP and dual-luciferase reporter assays. The experimental results confirmed the hypothesis, demonstrating that circEFR3A acts as a molecular sponge for miR-590-3p. Overexpression of circEFR3A was revealed to counteract miR-590-3p-mediated suppression, thereby promoting BC cell proliferation, migration and invasion.

Previous studies have reported that miR-590-3p serves a suppressive role in the pathogenesis of several cancers. For example, miR-590-3p was downregulated in tissues from 15 glioblastoma multiforme (GBM) cases and in five cell lines, where it inhibits GBM metastasis and epithelial-mesenchymal transition (EMT) by targeting zinc finger E-box binding homeobox 1/2 (32). In hepatocellular carcinoma, miR-590-3p suppresses cancer cell proliferation and migration, inhibits the expression of EMT-related genes by targeting mouse double minute 2 (33) and exerts tumor-suppressive effects by targeting TEA domain transcription factor 1 (34). A recent study also reported that the checkpoint suppressor 1/miR-590-3p/transcriptional co-activator with PDZ-binding motif axis contributes to multiple myeloma (35). In BC, miR-590-3p has been reported to participate in the antiproliferative effects of lutein through targeting cancer susceptibility 9 (36). Similarly, miRNA-590-3p inhibits invasion and metastasis in triple-negative BC by targeting Slug (37). Additionally, LINC00657 can act as a molecular sponge for miR-590-3p, serving a biological role in BC by regulating the miR-590-3p/golgi phosphoprotein 3 axis (38). Consistent with these aforementioned findings, in the present study, miR-590-3p inhibited the proliferation, migration and invasion of BC cells. Typically, the canonical mode of miRNA action involves direct binding to the 3'UTR of target genes, leading to their post-transcriptional repression or degradation. The present study employed the miRPathDB database to analyze the enrichment of post-translational protein modification pathways associated with miR-590-3p. Using databases such as TargetScan, GeneCards and miRPathDB, common target genes for miR-590-3p were predicted, with AR selected as a potential target. Through dual-luciferase reporter assays and western blotting, the hypothesis was also assessed at several levels. To the best of our knowledge, the present study is the first to demonstrate that the circRNA, circEFR3A, can act as a molecular sponge for miR-590-3p, exerting biological functions by regulating the miR-590-3p/AR signaling axis, thereby expanding the present understanding of the molecular mechanisms involved in the onset and progression of BC.

The expression rate of AR in BC ranges from 53-99%, with ~90% of ER-positive and ~20% of ER-negative BC exhibiting positive AR expression (39). Previous studies have reported that using 1% positive expression as a threshold, AR can serve as a marker of poor prognosis in triple-negative BC (40,41). Additionally, the AR antagonist MDV3100 can inhibit the growth of xenograft tumors in nude mice derived from AR-positive BC cells (41). AR antagonists are being used as treatment drugs for advanced triple-negative BC in phase II clinical trials, although their effectiveness has been unsatisfactory (42-44). Studying the interaction mechanisms between circRNA and AR holds practical significance for patients with AR-positive BC.

The results of the present study suggested that circEFR3A may regulate BC progression through the miR-590-3p/AR axis. However, it has remained unclear whether circEFR3A regulates tumor progression via other mechanisms. A total of 6 potential target genes were identified in the intersection of online database predictions. However, the present study did not investigate target genes other than AR. In parallel experiments performed by members of the present research group (unpublished data), transfection of the AR overexpression plasmid in BC cell lines resulted in a marked increase in circEFR3A expression. This observation led to the hypothesis that AR may act as a transcription factor to promote circEFR3A expression. When combined with the miR-590-3p/AR axis effect observed in the present study, we hypothesized that a positive feedback loop may exist between circEFR3A and AR. These speculations all present potential directions for future research. Consequently, the role of circEFR3A in BC warrants further investigation.

Prior to the present study, circEFR3A had not been widely reported based on our initial literature search. However, during the experimental phase of the present research, a published study was identified demonstrating that circEFR3A can upregulate EFR3A by binding with miR-654-3p, thereby promoting proliferation and migration in nasopharyngeal carcinoma cells (45). This corroborates the oncogenic role of circEFR3A in BC as observed in the present study.

However, there are several limitations of the present study. First, the present study does not fully assess whether circEFR3A interacts with other miRNAs or proteins. Future research should further validate other miRNAs and design circEFR3A RNA pull-down probes to perform RNA pull-down combined with proteomics analysis to evaluate whether it interacts with proteins to exert its function. Second, all tissues in the breast cancer tissue microarray were sourced from mainland China, and there is a lack of information regarding patient ethnicity, genetic background and Ki-67 index. This restricts the generalizability of the research findings and the understanding of tumor heterogeneity. Finally, in the animal experiments, there were 4 animals per group. Although studies with similar sample sizes were identified, a larger sample size would contribute to enhancing the statistical power and reliability of the results. considering the inherent differences among animals.

In conclusion, the results of the present study indicate that high expression of circEFR3A in BC tissues is associated with poor prognosis. Moreover, circEFR3A was revealed to promote the proliferation, migration and invasion of BC cells. Mechanistically,

circEFR3A acts as a molecular sponge for miR-590-3p, restoring the miR-590-3p-mediated targeting suppression of AR in BC cell lines. These research findings provide new molecular evidence that circEFR3A exerts its biological functions in BC through the miR-590-3p/AR axis. In the future, the combined application of circEFR3A inhibitors and AR antagonists may become a novel strategy for BC treatment.

**Acknowledgements**

Not applicable.

**Funding**

The present work was supported by the Medical Science Research Project of Hebei (grant no. 20240928).

**Availability of data and materials**

The data generated in the present study may be requested from the corresponding author.

**Authors' contributions**

YM and XW designed and performed the experiments. HS, ZW, SL, FL, WL and MS performed the data analysis and animal experiments, and contributed towards writing manuscript. CG conceptualized the design of the study, supplied resources and obtained the necessary funding. YM and XW confirm the authenticity of all the raw data. All authors read and approved the final manuscript.

**Ethical approval and consent to participate**

The present study was approved by the Research Ethics Committee of The Fourth Hospital of Hebei Medical University [approval nos. 2024KS189 (human ethics) and 2023016 (animal ethics)]. The ethical approval for the breast cancer tissue chip was provided by the Ethics Committee of Shanghai Outdo Biotech Company Co., Ltd. (approval no. SHYJS-BC-2310001).

**Patient consent for publication**

Not applicable.

**Competing interests**

The authors declare that they have no competing interests.

**References**

1. Fillon M: Breast cancer recurrence risk can remain for 10 to 32 years. CA Cancer J Clin 72: 197-199, 2022.
2. Siegel RL, Giaquinto AN and Jemal A: Cancer statistics, 2024. CA Cancer J Clin 74: 12-49, 2024.
3. Cardoso F, Paluch-Shimon S, Senkus E, Curigliano G, Aapro MS, André F, Barrios CH, Bergh J, Bhattacharyya GS, Biganzoli L, *et al*: 5th ESO-ESMO international consensus guidelines for advanced breast cancer (ABC 5). Ann Oncol 31: 1623-1649, 2020.
4. Klinge CM: Non-Coding RNAs in breast cancer: Intracellular and intercellular communication. Noncoding RNA 4: 40, 2018.
5. Qu S, Yang X, Li X, Wang J, Gao Y, Shang R, Sun W, Dou K and Li H: Circular RNA: A new star of noncoding RNAs. Cancer Lett 365: 141-148, 2015.
6. Memczak S, Jens M, Elefsinioti A, Torti F, Krueger J, Rybak A, Maier L, Mackowiak SD, Gregersen LH, Munschauer M, *et al*: Circular RNAs are a large class of animal RNAs with regulatory potency. Nature 495: 333-338, 2013.
7. Hansen TB, Jensen TI, Clausen BH, Bramsen JB, Finsen B, Damgaard CK and Kjems J: Natural RNA circles function as efficient microRNA sponges. Nature 495: 384-388, 2013.
8. Lei M, Zheng G, Ning Q, Zheng J and Dong D: Translation and functional roles of circular RNAs in human cancer. Mol Cancer 19: 30, 2020.
9. Zhou WY, Cai ZR, Liu J, Wang DS, Ju HQ and Xu RH: Circular RNA: metabolism, functions and interactions with proteins. Mol Cancer 19: 172, 2020.
10. Yu Y, Zheng W, Ji C, Wang X, Chen M, Hua K, Deng X and Fang L: Tumor-Derived circRNAs as circulating biomarkers for breast cancer. Front Pharmacol 13: 811856, 2022.
11. Yang B, Wang YW and Zhang K: Interactions between circRNA and protein in breast cancer. Gene 895: 148019, 2024.
12. Zhu J, Li Q, Wu Z, Xu W and Jiang R: Circular RNA-mediated miRNA sponge & RNA binding protein in biological modulation of breast cancer. Noncoding RNA Res 9: 262-276, 2024.
13. Gopikrishnan M, R HC, R G, Ashour HM, Pintus G, Hammad M, Kashyap MK, C GPD and Zayed H: Therapeutic and diagnostic applications of exosomal circRNAs in breast cancer. Funct Integr Genomics 23: 184, 2023.
14. Gao D, Cui C, Jiao Y, Zhang H, Li M, Wang J and Sheng X: Circular RNA and its potential diagnostic and therapeutic values in breast cancer. Mol Biol Rep 51: 258, 2024.
15. Weidle UH, Hsia HE and Brinkmann U: Breast cancer: Circular RNAs mediating efficacy in preclinical in vivo models. Cancer Genomics Proteomics 20: 222-238, 2023.
16. Liang G, Ling Y, Mehrpour M, Saw PE, Liu Z, Tan W, Tian Z, Zhong W, Lin W, Luo Q, *et al*: Autophagy-associated circRNA circCDYL augments autophagy and promotes breast cancer progression. Mol Cancer 19: 65, 2020.
17. Wu S, Lu J, Zhu H, Wu F, Mo Y, Xie L, Song C, Liu L, Xie X, Li Y, *et al*: A novel axis of circKIF4A-miR-637-STAT3 promotes brain metastasis in triple-negative breast cancer. Cancer Lett 581: 216508, 2024.
18. Fu B, Liu W, Zhu C, Li P, Wang L, Pan L, Li K, Cai P, Meng M, Wang Y, *et al*: Circular RNA circBCBM1 promotes breast cancer brain metastasis by modulating miR-125a/BRD4 axis. Int J Biol Sci 17: 3104-3117, 2021.
19. Ju C, Zhou M, Du D, Wang C, Yao J, Li H, Luo Y, He F and He J: EIF4A3-mediated circ_0042881 activates the RAS pathway via miR-217/SOS1 axis to facilitate breast cancer progression. Cell Death Dis 14: 559, 2023.
20. Song H, Zhao Z, Ma L, Zhao W, Hu Y and Song Y: Novel exosomal circEGFR facilitates triple negative breast cancer autophagy via promoting TFEB nuclear trafficking and modulating miR-224-5p/ATG13/ULK1 feedback loop. Oncogene 43: 821-836, 2024.
21. Livak KJ and Schmittgen TD: Analysis of relative gene expression data using real-time quantitative PCR and the 2(-Delta Delta C(T)) Method. Methods 25: 402-408, 2001.
22. Stelzer G, Rosen N, Plaschkes I, Zimmerman S, Twik M, Fishilevich S, Stein TI, Nudel R, Lieder I, Mazor Y, *et al*: The genecards suite: From gene data mining to disease genome sequence analyses. Curr Protoc Bioinformatics 54: 1 30 1-1 30 33, 2016.
23. Witkos TM, Koscianska E and Krzyzosiak WJ: Practical aspects of microRNA target prediction. Curr Mol Med 11: 93-109, 2011.
24. Kristensen LS, Andersen MS, Stagsted LVW, Ebbesen KK, Hansen TB and Kjems J: The biogenesis, biology and characterization of circular RNAs. Nat Rev Genet 20: 675-691, 2019.
25. Dolgin E: Why rings of RNA could be the next blockbuster drug. Nature 622: 22-24, 2023.
26. Liu CX and Chen LL: Circular RNAs: Characterization, cellular roles, and applications. Cell 185: 2390, 2022.
27. Zhang Y, Zhang X, Xu Y, Fang S, Ji Y, Lu L, Xu W, Qian H and Liang ZF: Circular RNA and its roles in the occurrence, development, diagnosis of cancer. Front Oncol 12: 845703, 2022.
28. Trybus M, Hryniewicz-Jankowska A, Wojtowicz K, Trombik T, Czogalla A and Sikorski AF: EFR3A: A new raft domain organizing protein?. Cell Mol Biol Lett 28: 86, 2023.
29. Gupta AR, Pirruccello M, Cheng F, Kang HJ, Fernandez TV, Baskin JM, Choi M, Liu L, Ercan-Sencicek AG, Murdoch JD, *et al*: Rare deleterious mutations of the gene EFR3A in autism spectrum disorders. Mol Autism 5: 31, 2014.

30. Hu H, Ye B, Zhang L, Wang Q, Liu Z, Ji S, Liu Q, Lv J, Ma Y, Xu Y, *et al*: Efr3a insufficiency attenuates the degeneration of spiral ganglion neurons after hair cell loss. Front Mol Neurosci 10: 86, 2017.
31. Adhikari H, Kattan WE, Kumar S, Zhou P, Hancock JF and Counter CM: Oncogenic KRAS is dependent upon an EFR3A-PI4KA signaling axis for potent tumorigenic activity. Nat Commun 12: 5248, 2021.
32. Pang H, Zheng Y, Zhao Y, Xiu X and Wang J: miR-590-3p suppresses cancer cell migration, invasion and epithelial-mesenchymal transition in glioblastoma multiforme by targeting ZEB1 and ZEB2. Biochem Biophys Res Commun 468: 739-745, 2015.
33. Youssef AI, Khaled GM and Amleh A: Functional role and epithelial to mesenchymal transition of the miR-590-3p/MDM2 axis in hepatocellular carcinoma. BMC Cancer 23: 396, 2023.
34. Ge X and Gong L: MiR-590-3p suppresses hepatocellular carcinoma growth by targeting TEAD1. Tumour Biol 39: 1010428317695947, 2017.
35. Bruno T, Catena V, Corleone G, Cortile C, Cappelletto MC, Bellei B, De Nicola F, Amadio B, Gumenyuk S, Marchesi F, *et al*: Che-1/miR-590-3p/TAZ axis sustains multiple myeloma disease. Leukemia 38: 877-882, 2024.
36. Zhang Y, Chang J, Jiang W, Ye X and Zhang S: Long non-coding RNA CASC9/microRNA-590-3p axis participates in lutein-mediated suppression of breast cancer cell proliferation. Oncol Lett 22: 544, 2021.
37. Yan M, Ye L, Feng X, Shi R, Sun Z, Li Z and Liu T: MicroRNA-590-3p inhibits invasion and metastasis in triple-negative breast cancer by targeting Slug. Am J Cancer Res 10: 965-974, 2020.
38. Shan Q, Qu F, Yang W and Chen N: Effect of LINC00657 on apoptosis of breast cancer cells by regulating miR-590-3p. Cancer Manag Res 12: 4561-4571, 2020.
39. Ricciardelli C, Bianco-Miotto T, Jindal S, Butler LM, Leung S, McNeil CM, O'Toole SA, Ebrahimie E, Millar EKA, Sakko AJ, *et al*: The magnitude of androgen receptor positivity in breast cancer is critical for reliable prediction of disease outcome. Clin Cancer Res 24: 2328-2341, 2018.
40. Bhattarai S, Klimov S, Mittal K, Krishnamurti U, Li XB, Oprea-Ilies G, Wetherilt CS, Riaz A, Aleskandarany MA, Green AR, *et al*: Prognostic role of androgen receptor in triple negative breast cancer: A multi-institutional study. Cancers (Basel) 11: 995, 2019.
41. Sang M, Meng L, Ma C, Liu S, Sang M, Chang S, Liu F, Lian Y and Geng C: Effect of AR antagonist combined with PARP1 inhibitor on sporadic triple-negative breast cancer bearing AR expression and methylation-mediated BRCA1 dysfunction. Biomed Pharmacother 111: 169-177, 2019.
42. Traina TA, Miller K, Yardley DA, Eakle J, Schwartzberg LS, O'Shaughnessy J, Gradishar W, Schmid P, Winer E, Kelly C, *et al*: Enzalutamide for the treatment of androgen receptor-expressing triple-negative breast cancer. J Clin Oncol 36: 884-890, 2018.
43. Bonnefoi H, Grellety T, Tredan O, Saghatchian M, Dalenc F, Mailliez A, L'Haridon T, Cottu P, Abadie-Lacourtoisie S, You B, *et al*: A phase II trial of abiraterone acetate plus prednisone in patients with triple-negative androgen receptor positive locally advanced or metastatic breast cancer (UCBG 12-1). Ann Oncol 27: 812-818, 2016.
44. Liu Y, Zhu XZ, Xiao Y, Wu SY, Zuo WJ, Yu Q, Cao AY, Li JJ, Yu KD, Liu GY, *et al*: Subtyping-based platform guides precision medicine for heavily pretreated metastatic triple-negative breast cancer: The FUTURE phase II umbrella clinical trial. Cell Res 33: 389-402, 2023.
45. Jiang P and Xia B: Circular RNA EFR3A promotes nasopharyngeal carcinoma progression through modulating the miR-654-3p/EFR3A axis. Cell Mol Biol (Noisy-le-grand) 69: 111-117, 2023.